

Micaceous Sands: Microscale Mechanisms and Macroscale Response

Jong-Sub Lee¹; Maria Guimaraes²; and J. Carlos Santamarina³

Abstract: The presence of mica changes the mechanical behavior of sandy soils. In this study, micro- and macroscale tests are used to explore the unique packing characteristics that develop in mixtures made of round and platy particles, and the effects that mica exerts on small, medium, and large strain parameters. Mixtures are prepared with different mica contents and various mica-to-sand size ratios, $L_{\text{mica}}/D_{\text{sand}}$. Results provide a comprehensive characterization of mixtures made of spherical and platy particles. Mica plates change sand packing through pore filling, bridging, ordering, and mica-mica interaction; bridging prevails and leads to open fabrics when $L_{\text{mica}}/D_{\text{sand}} \geq 1$. As the mica content increases in mixtures with $L_{\text{mica}}/D_{\text{sand}} \geq 1$, the shear-wave velocity decreases and it becomes more sensitive to the state of stress; the constraint modulus decreases; and the peak and residual friction angles decrease. Remixing during disordered granular flow prevents mica alignment and diminishes the otherwise weakening effect of mica on large-strain strength.

DOI: 10.1061/(ASCE)1090-0241(2007)133:9(1136)

CE Database subject headings: Compression; Density; Fabrics; Localization; Residual soils; Sand; Shear modulus; Stiffness.

Introduction

Residual soils are formed by the in situ weathering of rocks, and are composed of the same minerals forming the parent rock as well as new minerals that result from the weathering processes. For example, residual soils derived from granite contain the original minerals feldspar, quartz, and biotite, and newly formed minerals such as kaolinite, chlorite, and muscovite. The mica content in residual soils from weathered granite generally ranges between 0 and 20%, although values in excess of 75% have been reported for residual soils in Ghana (de Graft-Johnson et al. 1969; Gidigas 1976).

Crushed or “manufactured” sands may also contain mica. In this case, the amount of mica depends on the parent rock and ranges between 0 and 15% in crushed granite (Wood and Marek 1995). The potential utilization of manufactured sands and pond screenings depends in part on the effects of mica on material properties.

The presence of platy mica particles in sands affects grain packing. The packing of spherical particles has been the subject of intensive research in powder technology, physics, mathematics, and chemistry since the early 1600s (Fraser 1935; Scott 1960; Gray 1969; Cumberland and Crawford 1987). This line of re-

search has involved monosize and multisize spherical particles (Furnas 1931; Carman 1937; White and Walton 1937; German 1989). Contrary to the packing of spheres, the packing of non-spherical particles is largely empirical (Shergold 1953; Gray 1969; Youd 1973; Cumberland and Crawford 1987; German 1989). Early experimental data gathered with nearly spherical (lead shot) to platy particles (crushed mica) show that porosity increases considerably as sphericity decreases (Fraser 1935).

The mechanical response of soils is affected by the presence of mica as well. In particular, previous studies have shown that mica:

- Increases the compressibility of sandy soils and hinders compaction (Gilboy 1928; McCarthy and Leonard 1963; de Graft-Johnson et al. 1969; Moore 1971; Harris et al. 1984);
- Alters internal shear mechanisms from turbulent shear when the dominant particle shape is spherical (regardless of the coefficient of interparticle friction), to sliding shear when the dominant particle shape is platy and the coefficient of interparticle friction is low (Lupini et al. 1981);
- Decreases the strength to a low asymptotic value when the mica content reaches ~15% (Harris et al. 1984); and
- Causes significant undrained strength anisotropy from a brittle response in triaxial extension to a ductile behavior in triaxial compression (Hight et al. 1998).

Therefore, micaceous soils are often deemed unacceptable for embankment construction. Furthermore, a number of slope failures on residual soils have been attributed to the presence of mica (de Graft-Johnson et al. 1969; Harris et al. 1984; Hight et al. 1998).

Most prior studies have addressed the effects of mica content ($\% \text{mica} = W_{\text{mica}}/W_{\text{soil}} \times 100$) but have not explored the effects of relative size $L_{\text{mica}}/D_{\text{sand}}$ (see Table 1). The following experimental study is designed to investigate the impact of both ratios on particle packing and the mechanical response at small-to-large strains.

¹Assistant Professor, Dept. of Civil, Environmental and Architectural Engineering, Korea Univ., Seoul 136-701, Korea.

²Research Engineer, Aalborg Portland, Aalborg, Denmark.

³Professor, Dept. of Civil and Environmental Engineering, Georgia Institute of Technology, Atlanta, GA 30332.

Note. Discussion open until February 1, 2008. Separate discussions must be submitted for individual papers. To extend the closing date by one month, a written request must be filed with the ASCE Managing Editor. The manuscript for this paper was submitted for review and possible publication on July 18, 2005; approved on November 6, 2006. This paper is part of the *Journal of Geotechnical and Geoenvironmental Engineering*, Vol. 133, No. 9, September 1, 2007. ©ASCE, ISSN 1090-0241/2007/9-1136-1143/\$25.00.

Table 1. Relative Size and Mica Content Used in Experimental Studies by Previous Researchers

Reference	$L_{\text{mica}}/D_{\text{sand}}$	Mica content by weight (%)
Gilboy (1928)	Cannot be inferred from data	0, 5, 10, 20, 40
McCarthy and Leonard (1963)	1–5	0, 3, 6, 12, 25, 50, 100
de Graft-Johnson et al. (1969) ^a	Cannot be inferred from data	0, 56, 68, 77, 84
Moore (1971)	0.48–2	0, 5, 10, 30, 50, 100
Harris et al. (1984)	~1.7	0, 5, 10, 15, 25, 50
Lupini et al. (1981)	0.03–1.5	0, 25, 40, 60, 70, 100
Hight et al. (1998)	~0.67	0, 1, 2.5, 10, 20, 40
This study	0.33, 0.66, 1, 2, 3	0, 1, 2, 5, 10, 20, 100

^aNatural sand.

Particle-Level Packing Phenomena

Mica particles are thin flat plates that promote the organized packing or “ordering” of round particles above them when particles are allowed to reach their minimum potential energy configuration during slow sedimentation. Tetrahedral and loose simple cubic packings can form depending on the plane inclination α , as shown in Fig. 1 (Fraser 1935; Graton and Fraser 1935; Gray 1969). On the lower side, platy mica particles may bridge over voids left by the underlying round particles (Fig. 1). The impact of ordering above and bridging below mica particles is related to the relative size between platy and spherical particles $L_{\text{mica}}/D_{\text{sand}}$. These packing effects are further studied next.

Ordering (above Platy Particles)

A two-dimensional physical model is used to study the region where packing is affected by the presence of short planar interfaces. The experimental setup consists of monosize disks (1 cent U.S. coins: 19 mm diameter D and 1.5 mm thick) and flat bars (1.8 mm high, 1.8 mm thick, various lengths L ; aluminum) placed between two Plexiglas plates (600 mm wide, 350 mm high, and at 2 mm separation). The monosize disks are pluviated into the slot. A limited number of flat bars are also rained in. Typically, these bars sit at angles that range between $\alpha = \pm 35^\circ$. The tested size ratios are $L/D = 3, 5, \text{ and } 10$.

For the given flat bar, the packing of disks above the bar is recorded using a transparent paper. First, the bar drawn on the paper is carefully aligned with the bar under study. Then, the center of each disk is recorded on the transparent paper. Ten records are superimposed on each plot, shown in Fig. 2: each point documents the center of a disk. Disk centers appear at well-defined locations immediately above the flat bars, whereas random locations are recorded at greater distances away from the bars. The parabolic lines sketched in Fig. 2 suggest the boundaries

for the zones above the flat bars where the packing of the disks is affected by the presence of the planar inclusions.

The number of disk centers within a bin is counted as the bin is moved away from the bar. The resulting spatial histograms are shown on the rights in Fig. 2. The peaks in the distributions take place at characteristic distances away from the flat bars. Circles of the same size as the coins are sketched in the upper part of Fig. 2, aligning the centers with the frequency peaks. These results suggest that round disks tend to form a tetrahedral arrangement above the platy particles. [Note: the effect of angular particles is unknown in this case; however, published data by Cho et al. (2006) show that angularity and roughness promote looser packing configurations.]

The amplitude of the peaks decays away from the plates as the fabric becomes less regular. The influence length for each L/D condition is determined by the area where large peaks can be identified. The influence length does not exceed five particle diameters ($5D$ for $L/D = 10$) and it decreases as L/D decreases (the influence length is almost $3D$ for $L/D = 3$).

Bridging (below Platy Particles)

Platy particles may form bridges over round particles and cause an increase in mixture porosity. Relative size $L_{\text{mica}}/D_{\text{sand}}$ and the type of rotund particle packing (either loose or dense) determine the impact of bridging on mixture porosity. This is demonstrated with sketches in Fig. 3.

Simple volumetric analyses predict that the void ratio increases with mica content. However, there is a tradeoff between size ratio $L_{\text{mica}}/D_{\text{sand}}$ and number of particles (for the same mica content and slenderness): as the size ratio $L_{\text{mica}}/D_{\text{sand}}$ increases, the number of mica particles in the mixture decreases, and hinders the impact of bridging on global porosity.

Combined Effects of Ordering and Bridging: Packing Density

Mixtures of mica and Ottawa sand are prepared to cover size ratios $L_{\text{mica}}/D_{\text{sand}} = 0.33, 0.66, 1, 2, \text{ and } 3$ and mica fractions %mica = 0, 1, 2, 5, 10, 20, and 100% (for comparison, the size ratios and mica fractions studied by previous researchers are summarized in Table 1). Ottawa 20–30 sand is used for mixtures with size ratios $L_{\text{mica}}/D_{\text{sand}} \leq 1$, while Ottawa 50–70 is used for mixtures with $L_{\text{mica}}/D_{\text{sand}} \geq 1$. The mica flakes are commercially available crushed muscovite (V-115, Oglebay Norton Minerals, Cleveland, Ohio). The different sizes are obtained by dry sieving.

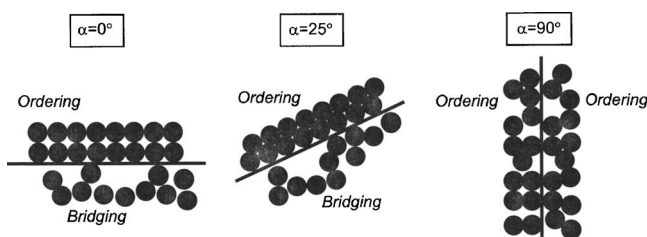


Fig. 1. Hypothesized bridging and ordering effects: Platy particle orientation α

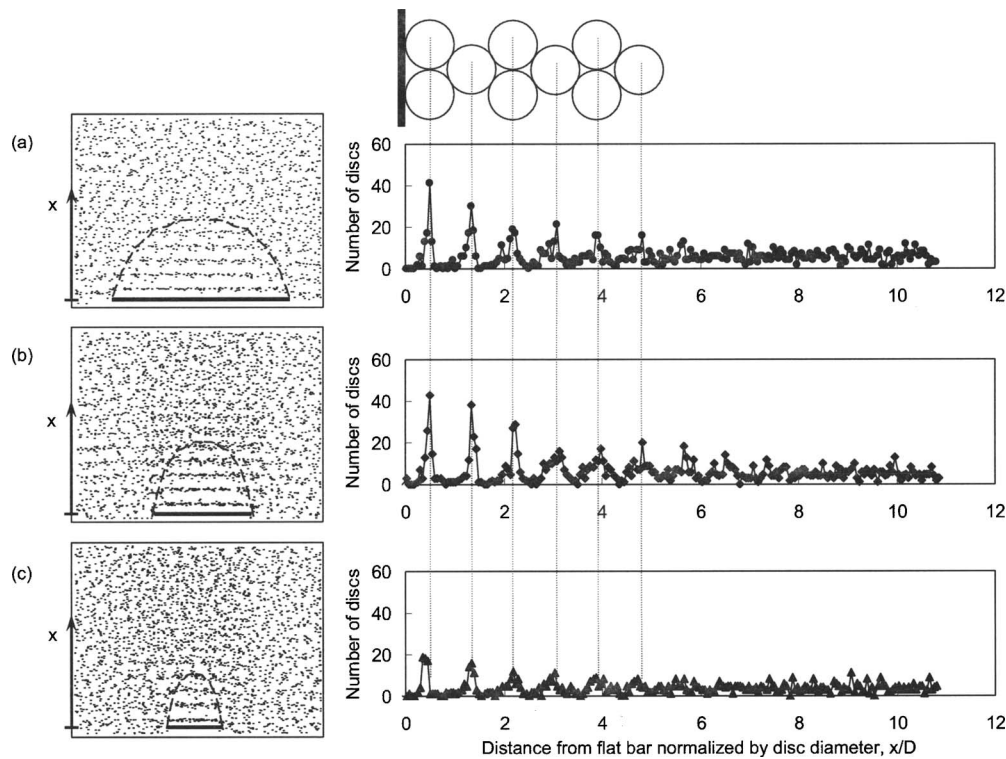


Fig. 2. Particle ordering above flat bars. Relative sizes: (a) $L/D=10$; (b) $L/D=5$; (c) $L/D=3$. Figures on left: each point indicates the center of a disk (10 cases are superimposed on each figure); the parabolic lines suggest the approximate boundary between regular packing and random packing. Figures on right: corresponding spatial histograms.

The geometric and packing characteristics of these materials are summarized in Table 2. Microphotographs of mica and Ottawa sand are presented in Fig. 4.

The depositional method plays an important role in the type of packing and homogeneity of these mixtures. Several specimen

preparation methods were tested as part of this study. We selected the funneling of uniform mixtures because it produces the most homogeneous specimens.

The uniform mixtures are funneled into 50 mL graduated cylinders to study loose packing conditions. Fig. 5 shows the variation in measured void ratio. In general, the void ratio increases with increasing mica content. However, mixtures with size ratios $L_{mica}/D_{sand}=0.33$ and 0.66 do not change the void ratio at low %mica; in fact, small mica flakes may fill the voids left between sand particles and cause a decrease in void ratio. Bridging effects prevail in mixtures with size ratio $L_{mica}/D_{sand} \geq 1$ even at low mica content (%mica < 5%). At high mica content (>5%), differences in size ratio diminish due to the fewer numbers of mica particles in mixtures with large L_{mica}/D_{sand} ratios, and mutual interaction between mica particles. In summary, the porosity in mi-

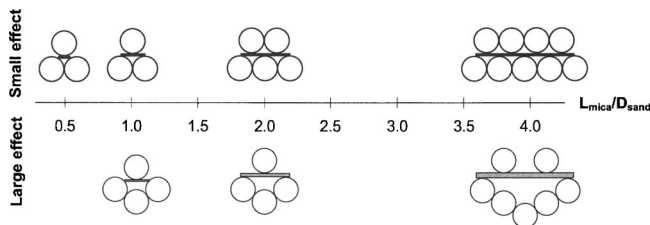


Fig. 3. Bridging: effect of relative size L_{mica}/D_{sand} on void ratio

Table 2. Characteristics of Tested Materials

Measurement	Ottawa 50–70	Ottawa 20–30	Mica (very fine)	Mica (fine)	Mica (medium)	Mica (medium)
D_{50} (cm)	0.025	0.073	—	—	—	—
L_{50} (cm)	—	—	0.01	0.033	0.051	0.073
Sphericity ^a	0.9	0.9	0.3 ^a	0.3 ^a	0.3 ^a	0.3 ^a
Roundness	0.5	0.7	0.1	0.1	0.1	0.1
G_s	2.65	2.65	2.82	2.82	2.82	2.82
e_{max}	0.85	0.74	NA	NA	NA	NA
e_{min}	0.59	0.50	NA	NA	NA	NA
Mineral	Quartz	Quartz	Muscovite	Muscovite	Muscovite	Muscovite

Note: NA=not available.

^aSphericity on the z-axis=0.9.

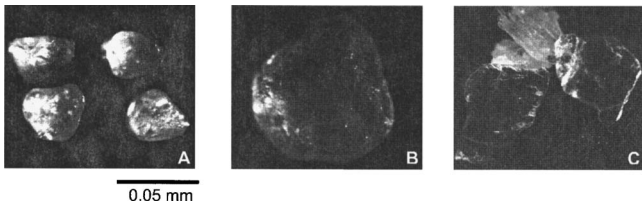


Fig. 4. Photomicrographs: (a) Ottawa Sand 50–70; (b) Ottawa Sand 20–30; and (c) mica

aceous sands combines pore filling ($L_{mica}/D_{sand} < 1$), bridging and ordering ($L_{mica}/D_{sand} \geq 1$), and mica–mica interaction effects ($\%mica > \sim 10\text{--}15\%$).

Small Strain: Shear-Wave Velocity

The effect of platy particles on the small strain stiffness of soils is tested by conducting shear-wave velocity-measurements in a conventional oedometer cell equipped with bender elements. The materials tested are mixtures of Ottawa 50–70 sand and different size mica flakes (Table 2): $\%mica=0$ (sand), 1, 5, 10, and 100% (mica) and size ratios $L_{mica}/D_{sand}=0.33, 1$, and 3. The oedometer cell is 105 mm in diameter and 80 mm in height. The uniform mixture (~ 350 g) is placed in five layers; each layer is funneled into the cell and lightly densified by pressing the layer once using a rod (weight: 650 g; diameter: 33 mm). The frequency response of bender elements ranges between 2 and 10 kHz depending on the material stiffness, and the corresponding range in wavelengths is

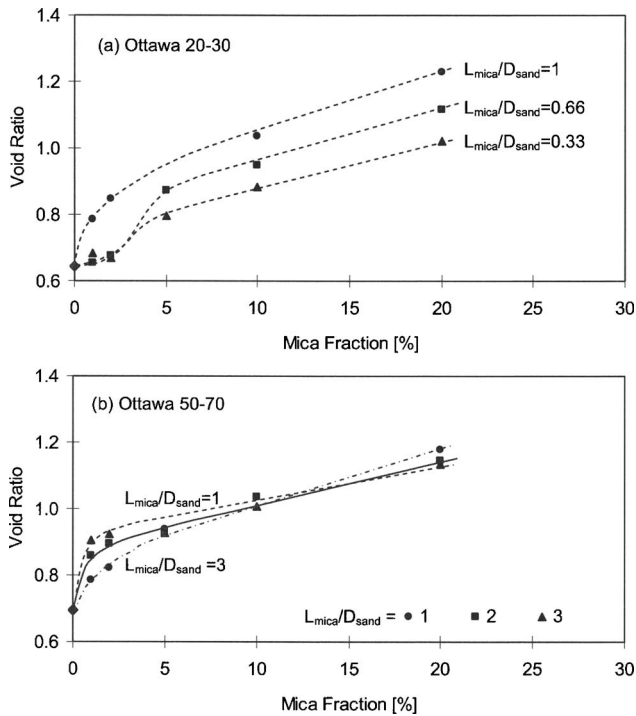
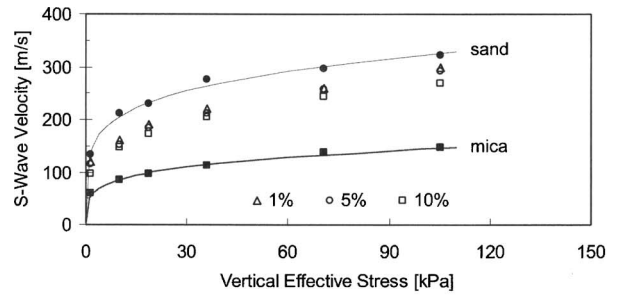
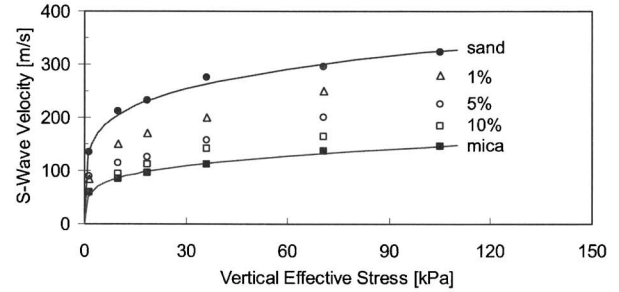


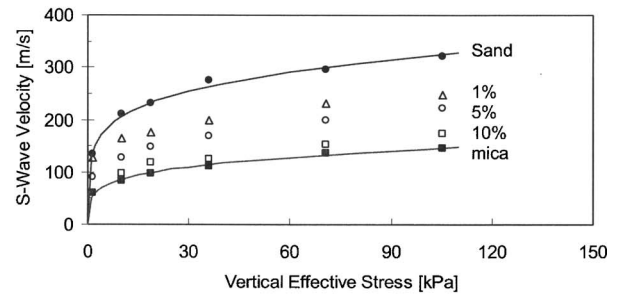
Fig. 5. Void ratio versus percentage mica for mixtures of sand. Data show the combined effects of filling (low L_{mica}/D_{sand}), ordering and bridging (for $L_{mica}/D_{sand} \geq 1$), and mica–mica interface (high $\%mica$): (a) Mixtures with Ottawa 20–30 sand; (b) mixtures with Ottawa 50–70 sand.



(a)



(b)



(c)

Fig. 6. Shear wave velocity data versus vertical effective stress for mixtures with Ottawa 50–70 sand with different amounts of mica: (a) $L_{mica}/D_{sand}=0.33$; (b) $L_{mica}/D_{sand}=1$; and (c) $L_{mica}/D_{sand}=3$. Numbers in the figure denote the mica content.

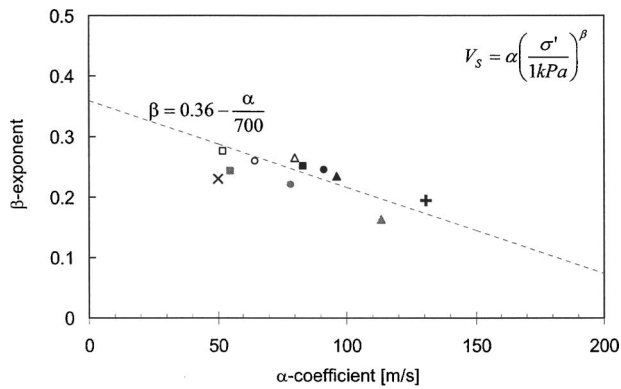
between 5 and 10 mm; therefore, the wavelength is much longer than the grains and data are analyzed using equivalent continuum wave propagation theory.

The shear-wave velocity is plotted versus vertical effective stress in Fig. 6. It is noted that: (1) the shear-wave velocity increases with the applied load; (2) the shear-wave velocity is higher in sand than in mica; (3) the softening effect of mica is small when $L_{mica}/D_{sand}=0.33$, confirming the pore-filling role of mica in this case; and (4) the shear-wave velocity decreases monotonically with mica content when the size ratio $L_{mica}/D_{sand} \geq 1$.

The shear-wave velocity reflects the stiffness of the skeleton G_{sk} and the density of the mixture ρ

$$V_S = \sqrt{\frac{G_{sk}}{\rho}} \quad \text{and} \quad G_{sk} = V_S^2 \cdot \rho \quad (1)$$

An increase in the applied load causes the stiffening of contacts and the increase in G_{sk} , but it also produces volume reduction and an increase in mass density ρ . In general, the increase in density is small even in high mica content mixtures, hence, V_S increases with confinement. The dependence of shear-wave velocity V_S



		Mica Content		
		1%	5%	10%
L_{mica}/D_{sand}	0.3	▲	●	■
	1	△	○	□
	3	▲	●	■
Extreme Values		+: 100% Sand	x: 100% Mica	

Fig. 7. Stress dependent velocity. Values of the α coefficient and β exponent in the velocity–stress power equation obtained by fitting shear-wave velocity data. The linear trend ($\beta=0.36-\alpha/700$), which is based on an extensive database that includes soft to stiff clays and dense-round to loose-angular sands, is adapted from Santamarina et al. (2001).

(m/s) on the applied load can be modeled with the semiempirical power equation

$$V_s = \alpha \left(\frac{\sigma'}{1 \text{ kPa}} \right)^\beta \quad (2)$$

The α coefficient is shear-wave velocity of the mixture (m/s) at an effective stress of $\sigma'=1$ kPa and it depends on the void ratio, fabric, and particle stiffness. The β exponent is related to the nature of contact stiffness and it is the slope of the shear-wave velocity versus stress plot in log–log scale. Fig. 7 presents the α coefficients and β exponents determined for all mixtures. Note that for a given L_{mica}/D_{sand} ratio, the β exponent increases and the α coefficient decreases as the mica content increases, in agreement with the softer and more stress-sensitive behavior of mica-ceous sands.

Simple structural models postulated based on common packings observed in the microscale experiments corroborate the high flexibility of beam elements, which is proportional to L^3 . Two-dimensional photoelastic tests with circular disks and different size flexible plates ($L/D=1-4$) show that the presence of flexible platy particles has a profound effect on the percolation of interparticle forces, which tend to arch around the flexible platelets [pictures can be founded in Guimaraes (2002)]. These two observations suggest that the decreased stiffness in mixtures reflects both the deformability of platy inclusions as well as the ensuing changes in internal force transmission.

Midstrain K_o Loading: Compression Index

Oedometer load–deformation data are analyzed to assess the effect of platy particles on the compression index. The following mixtures are tested: %mica=0 (sand), 1, 2, 5, 10, 20, and 100% (mica) for five different size ratios $L_{mica}/D_{sand}=0.33, 0.66, 1, 2,$

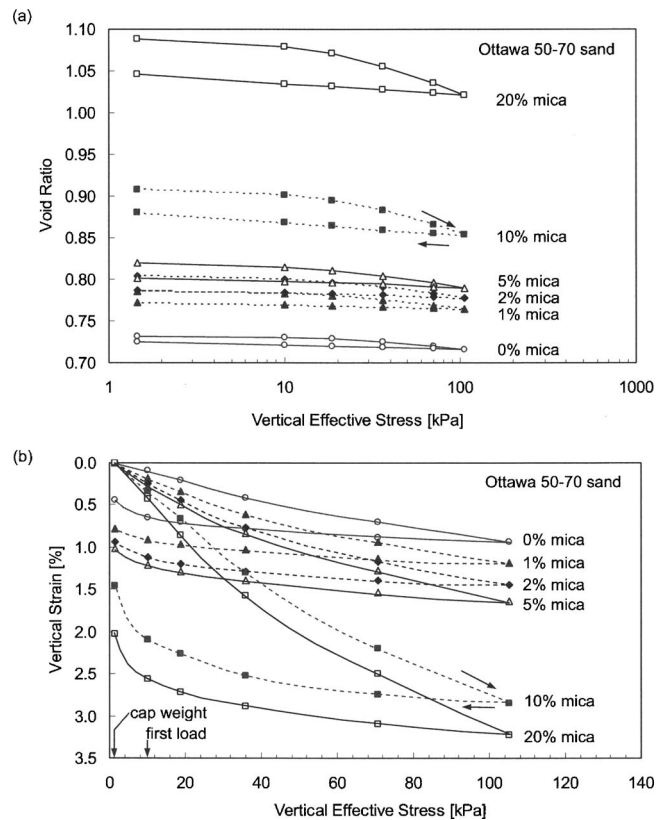


Fig. 8. Zero lateral strain load–deformation response for mixtures prepared with Ottawa 50–70 sand and mica. Size ratio $L_{mica}/D_{sand}=2$: (a) void ratio versus vertical effective stress (log scale); (b) vertical strain versus vertical effective stress (linear scale).

and 3 (Table 2). The cell and specimen preparation are as described in the previous section. A set of load–deformation trends is presented in Fig. 8 for $L_{mica}/D_{sand}=2$. The initial void ratio increases with increasing mica fraction due to bridging and ordering effects, as shown in Fig. 8(a). As the vertical effective stress increases, the reduction in void ratio increases with increasing mica fraction. Differences in load–deformation response are highlighted when results are presented in terms of strains [Fig. 8(b)]. Sieve data show no evidence of particle crushing in any of the specimens after unloading; apparently, high particle flexibility and interparticle force arching around soft zones help prevent particle breakage (note: limited crushing may not be detectable with this technique).

Fig. 9 shows the compression index C_c determined between $\sigma'=70-105$ kPa plotted versus mica fraction for all tested mixtures. The compression index increases with mica content once the mica content exceeds %mica > 2%; there is no clear effect of size ratio L_{mica}/D_{sand} on C_c .

Values of the compression index for sand–mica mixtures are plotted in Fig. 10, including results from this study and published data. In all cases, the compression index increases with mica content. Differences between values from different studies can be attributed to differences in materials and specimen preparation procedures [e.g., Gilboy (1928) aims to cause random orientation of mica flakes]. For comparison, the plot includes clay data: as observed by Terzaghi and Peck (1948), compressibility increases greatly with the presence of platy particles.

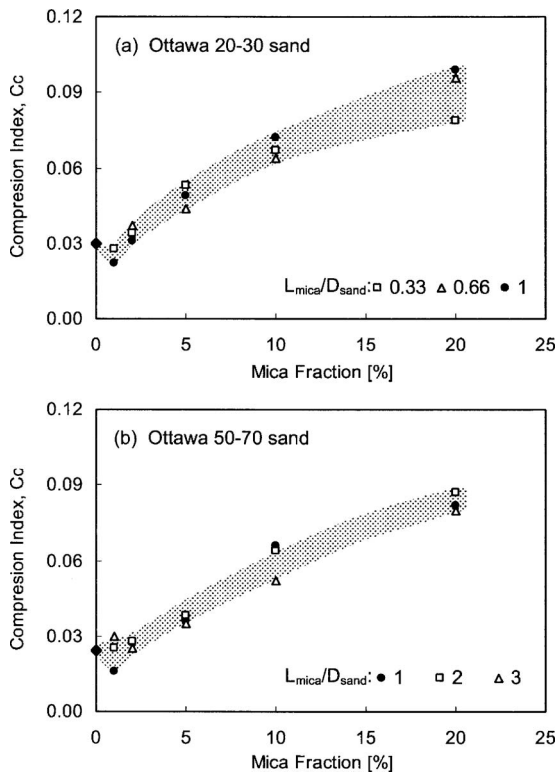


Fig. 9. Values of compression index C_c versus mica fraction %mica for different values of size ratio L_{mica}/D_{sand} : (a) mixtures with Ottawa 20–30 sand; (b) mixtures with Ottawa 50–70 sand

High Strain: Friction Angle

Drained triaxial compression tests are conducted using 35 mm diameter and 70 mm height specimens. To minimize segregation, the specimen is prepared in six layers by funneling 20 g of mixture at the time, and pressing the layer once using a rod (weight: 650 g; diameter: 33 mm). The deviatoric stress is applied under

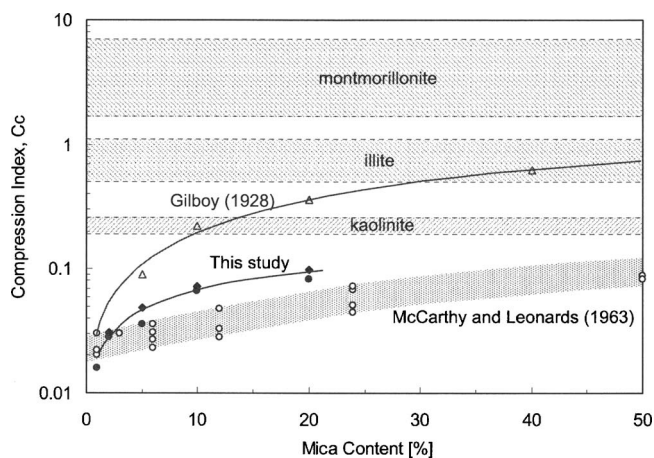


Fig. 10. Compression index values versus mica content. Data: Δ from Gilbo (1928); \circ from McCarthy and Leonard (1963) with size ratio $L_{mica}/D_{sand}=1.2-3$; \blacklozenge and \blacklozenge from this study (Ottawa 20–30 and 50–70 sand, both $L_{mica}/D_{sand}=1$). The range of values for kaolinite, illite, and montmorillonite are gathered from Lambe and Whitman (1979).

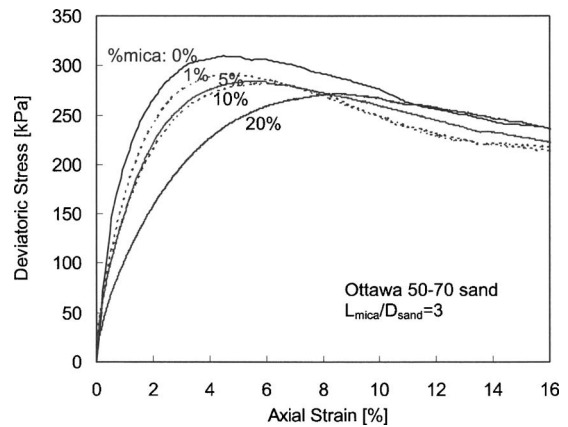


Fig. 11. Effect of mica content on the deviatoric stress versus axial strain response: drained triaxial tests at $\sigma'_c=80$ kPa

an effective confining pressure of 80 kPa. The maximum axial strain is 15%. Fig. 11 shows the deviatoric stress versus axial strain trends for mixtures with size ratio $L_{mica}/D_{sand}=3$. The peak strength decreases and the strain at peak strength is delayed with increasing mica content. The probability of localization also increases with mica content, and localization becomes inevitable when %mica \rightarrow 100%, even when the overall volume response is contractive (Santamarina and Cho 2003). Once again, sieve data gathered before and after loading show no evidence of particle crushing.

Values for the peak friction angle ϕ_p obtained from triaxial tests, plotted in Fig. 12(a), show a decrease with mica content (see also Lupini et al. 1981; Harris et al. 1984). Size ratio does not appear to have a significant influence on ϕ_p when $L_{mica}/D_{sand} > 1$.

The residual state friction angle ϕ_r is determined using a graduated cylinder. The selected mixture (~ 500 g) is poured in a 1,000 mL graduated cylinder filled with water. The cylinder is tilted passed 60° , and it is slowly brought back to the vertical position. The angle of repose is measured in the middle region of the slope (details in Santamarina and Cho 2001). For this test, mixtures are prepared with %mica=0 (sand), 1, 2, 5, 10, and 20% and size ratios $L_{mica}/D_{sand}=1$ and 3. Results in Fig. 12(b) show a decrease in ϕ_r with mica content in all cases (see also Lupini et al. 1981). The decrease in residual friction angle with mica content takes place between %mica=2 and 10, and it is more pronounced in ϕ_r than in ϕ_p .

Large strain leads to mica segregation in ring shear, i.e., rigid wedge slope failure. However, disordered landslide movement may force remixing. The effect of remixing is explored in an 80 mm diameter rotating chamber using ~ 100 g of mixture. The friction angle is measured at a constant angular velocity of 3 rpm. Results in Fig. 12(c) show that remixing hinders the weakening effect of mica on strength.

Particle alignment is expected when the strain level is about $\gamma \sim 50-100\%$ (residual). At larger strains, segregation takes place. How do round and platy grains segregate? Careful observation of the rotating cylinder experiments reveals segregation by differential mobility, particularly in large size ratio mixtures (e.g., $L_{mica}/D_{sand} \approx 3$), whereby platy particles can readily slide over the round particles. As segregation takes place, a continuous mica plain can form unless remixing is enforced as is the case in these rotational tests.

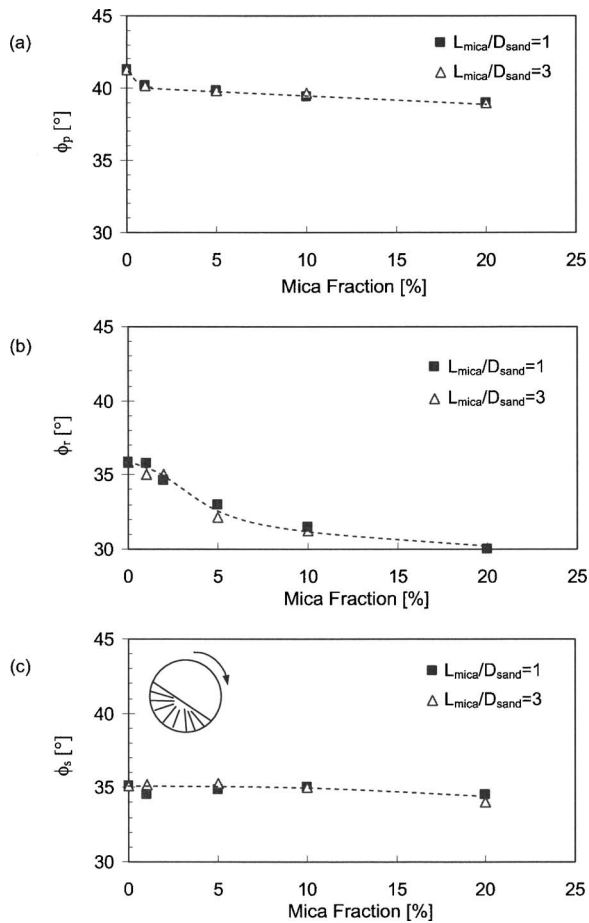


Fig. 12. Friction angle versus mica content for mixtures with different size ratios: (a) peak friction angle; (b) friction angle at residual state; and (c) friction angle at very large strains (with remixing)

Conclusions

Published results and new experimental evidence permit gaining a comprehensive understanding of mixtures made of spherical and platy particles, such as micaceous sands. The main observations are as follows:

- Mica flakes alter the packing of rounded particles through pore filling ($L_{mica}/D_{sand} < 1$), bridging and ordering effects ($L_{mica}/D_{sand} \geq 1$), and mica–mica interaction (high %mica). Both bridging and ordering depend on the orientation of platy particles. The length of influence for ordering effects is approximately equal to the length of mica flakes but not greater than five times the diameter of round particles. Bridging causes the increase in void ratio with increasing mica content when $L_{mica}/D_{sand} \geq 1$;
- Mica particles flex without crushing (within the tested stress range), cause the redistribution of interparticle forces, and soften the sand granular skeleton;
- The shear-wave velocity decreases with increasing mica content. Furthermore, the β exponent in the velocity–stress power equation increases with mica content, indicating higher stress sensitivity in the stiffness of micaceous sand;
- The compression index increases with mica content and it appears to be sensitive to the orientation of mica flakes, which is a consequence of the depositional method. While larger L_{mica}/D_{sand} ratios are more effective than smaller L_{mica}/D_{sand}

ratios at low mica content, size ratio has a limited impact on the compression index in part due to the tradeoff between the number of platy particles and the size ratio L_{mica}/D_{sand} for the same mica content %mica;

- The presence of platy mica particles delays the strain at peak strength and promotes shear strain localization; and
- The decrease in the residual friction angle with mica content is more pronounced than the decrease in the peak friction angle as the mica fraction exceeds 2%; size ratio plays a secondary role. Remixing during enforced disordered flow diminishes the effect of mica on strength.

Acknowledgments

This study was conducted while the writers were at the Georgia Institute of Technology, with support from Georgia mining companies and The Goizueta Foundation. Anonymous reviewers provided insightful comments and suggestions.

References

- Carman, P. C. (1937). "Fluid flow through granular beds." *Trans. Inst. Chem. Eng.*, 15, 150–166.
- Cho, G. C., Dodds, J., and Santamarina, J. C. (2006). "Particle shape effects on packing density, stiffness, and strength: Natural and crushed sands." *J. Geotech. Geoenviron. Eng.*, 132(5), 591–602.
- Cumberland, D. J., and Crawford, R. J. (1987). "The packing of particles." *Handbook of powder technology*, Vol. 6, Elsevier, New York.
- de Graft–Johnson, J. W. S., Bhatia, H. S., and Gidigas, D. M. (1969). "The strength characteristics of residual micaceous soils and their application to stability problems." *Proc., 7th Int. Conf. on Soil Mechanics and Foundation Engineering*, Mexico, 165–172.
- Fraser, H. J. (1935). "Experimental study of the porosity and permeability of clastic sediments." *J. Geol.*, 13(8), 910–1010.
- Furnas, C. C. (1931). "Grading aggregates I: Mathematical relations for beds for broken solids for maximum density." *Ind. Eng. Chem.*, 23(9), 1052–1058.
- German, R. M. (1989). *Particle packing characteristics*, Princeton University Press, Princeton N.J.
- Gidigas, M. D. (1976). *Laterite soil engineering*, Elsevier, Amsterdam, The Netherlands.
- Gilboy, G. (1928). "The compressibility of sand–mica mixtures." *Proc., American Society of Civil Engineering*, ACSE Transactions, 54, ASCE, New York, 555–568.
- Graton, L. C., and Fraser, H. J. (1935). "Systematic packing of spheres with particular relation to porosity and permeability." *J. Geol.*, 13(8), 785–909.
- Gray, W. A. (1969). *The packing of solid particles*, Chapman and Hall, London.
- Guimaraes, M. (2002). "Crushed stone fines and ion removal from clay slurries: Fundamental studies." Ph.D. thesis, Georgia Institute of Technology, Atlanta.
- Harris, W. G., Parker, J. C., and Zelazny, L. W. (1984). "Effects of mica content on the engineering properties of sand." *Soil Sci. Soc. Am. J.*, 48(3), 501–505.
- Hight, D. W., Georgiannou, V. N., Martin, P. L., and Mundegar, A. K. (1998). "Flow slides in micaceous sand." *Problematic soils*, Yanagisawa, E., Moroto, N., and Mitachi, T., eds., Baklema, Rotterdam, Sendai, Japan, 945–958.
- Lambe, T. W., and Whitman, R. V. (1979). *Soil mechanics—SI version*, Wiley, New York.
- Lupini, J. F., Skinner, A. E., and Vaughan, P. R. (1981). "The drained residual strength of cohesive soils." *Geotechnique*, 31(2), 181–213.

- McCarthy, D. F., and Leonard, R. J. (1963). "Compaction and compression characteristics of micaceous fine sands and silts." *Highway Research Record* 22, Transportation Research Board, Washington, D.C. 23–37.
- Moore, C. A. (1971). "Effect of mica on K_o compressibility of two soils." *J. Soil Mech. and Found. Div.*, 97(9), 1275–1291.
- Santamarina, J. C., and Cho, G. C. (2001). "Determination of critical state parameters in sandy soils—Simple procedure." *Geotech. Test. J.*, 24(2), 185–192.
- Santamarina, J. C., and Cho, G. C. (2003). "The omnipresence of localizations in particulate materials." *Deformation of characteristics of geomaterials*, H. Di Benedetto, T. Doanh, H. Geoffro, and C. Sauzeat, eds., Swets & Zeitlinger, Lisse, The Netherlands, 465–473.
- Santamarina, J. C., Klein, K., and Fam, M. (2001). *Soils and waves*, Wiley, Chichester, U.K.
- Scott, G. D. (1960). "Packing of spheres." *Nature (London)*, 188, 908–909.
- Shergold, F. A. (1953). "The percentage voids in compacted gravel as a measure of its angularity." *Mag. Concrete Res.*, 13, 3–10.
- Terzaghi, K., and Peck, R. B. (1948). *Soil mechanics in engineering practice*, Wiley, New York.
- White, H. E., and Walton, S. F. (1937). "Particle packing and particle shape." *J. Am. Ceram. Soc.*, 20(5), 155–166.
- Wood, S. A., and Marek, C. R. (1995). "Recovery and utilization of quarry by-products for use in highway construction." *Proc., 3rd Annual Center for Aggregate Research Symp.*, Univ. of Texas, Austin, Tex., 1–19.
- Youd, T. L. (1973). "Factors controlling maximum and minimum densities of sand." *Relative Density Involving Cohesionless Soils, ASTM-STP 523*, R. T. Selig and R. S. Ladd, eds., ASTM, Philadelphia, 98–112.